

Diamond Channel-Cut Crystals for High-Heat-Load, Beam-Multiplexing, Narrow-Band X-ray Monochromators

Yuri Shvyd'ko,^{1,*} Sergey Terentyev,² Vladimir Blank,² and Tomasz Kolodziej^{1,3}

¹*Advanced Photon Source, Argonne National Laboratory, Argonne, Illinois 60439, USA*

²*Technological Institute for Superhard and Novel Carbon Materials, 142190 Troitsk, Russian Federation*

³*National Synchrotron Radiation Centre SOLARIS, 30-392 Krakow, Poland*

Next-generation, high-brilliance x-ray photon sources call for new x-ray optics. Here we demonstrate the feasibility of using monolithic diamond channel-cut crystals as high-heat-load, beam-multiplexing, narrow-band, mechanically-stable x-ray monochromators with high-power x-ray beams at cutting-edge, high-repetition-rate x-ray free-electron laser (XFEL) facilities. The diamond channel-cut crystals fabricated and characterized in these studies are designed as two-bounce Bragg reflection monochromators directing 14.4-keV or 12.4-keV x-rays within a 15-meV-bandwidth to ⁵⁷Fe or ⁴⁵Sc nuclear resonant scattering experiments, respectively. The crystal design allows out-of-band x-rays within a $\simeq 1$ -eV XFEL bandwidth to be transmitted with minimal losses to alternative simultaneous experiments. Only $\lesssim 2\%$ of the incident $\simeq 100$ -W x-ray beam is absorbed in a 50- μm -thick first diamond crystal reflector, ensuring that the monochromator crystal is highly stable. Other x-ray optics applications of diamond channel-cut crystals are anticipated.

PACS numbers: 41.50.+h, 41.60.Cr, 61.05.cp

I. INTRODUCTION

Hard x-ray free-electron lasers (XFELs) in the self-seeding mode [1, 2] generate fully coherent brilliant x-ray beams with a well-defined and narrow spectrum, typically with a bandwidth of $\simeq 0.2 - 1$ eV [3–6] and a pulse duration of a few tens of femtoseconds.

When operated in a high-repetition-rate (\simeq MHz) pulse sequence mode with properly tapered undulators, self-seeded XFELs may deliver x-rays with a pulse energy of $\simeq 10$ mJ/pulse ($\simeq 7 \times 10^{12}$ photons/pulse of $\simeq 10$ -keV photons) and a time-averaged power of more than 100 W, corresponding to a time-averaged spectral flux of $\simeq 10^{17}$ photons/s in a bandwidth of $\lesssim 1$ eV [7]. This flux is about three orders of magnitude larger than the average spectral flux currently possible with storage ring-based synchrotron radiation sources [see also [8, 9]].

An x-ray source with an increase of three orders of magnitude in the spectral flux opens exciting new opportunities for hard x-ray spectroscopic techniques, such as inelastic x-ray scattering [10], x-ray photon correlation spectroscopy [11] and nuclear resonant scattering [12] in particular.

Such opportunities can be realized today, because high-repetition-rate hard x-ray XFELs are now a reality. The European XFEL in Hamburg (Germany) [13] is the first operational high-repetition-rate XFEL facility. The LCLS-II-HE in Stanford (USA) [14] is coming soon.

However, these new hard x-ray sources with high average spectral brilliance present not only opportunities but also challenges. One challenge is how to monochromatize XFEL beams of very high average and peak power.

To address these challenges, we have designed, manufactured and tested diamond channel-cut crystals for use as high-heat-load, beam-multiplexing, narrow-band (15-meV-bandwidth), mechanically-stable monochromators.

A schematic of our channel-cut crystal design together with relevant x-ray beams is shown in Fig. 1(a). We choose a channel-cut monolithic monocrystalline design for two reasons. First, this design enables multiple successive Bragg reflections (two, four, etc.) by perfectly aligned, parallel, mechanically stable reflecting atomic planes in the reflecting crystal plates P_1 and P_2 of the monolithic system. Second, it ensures parallel propagation of the incident and multiply reflected beams. The design includes a drumhead structure shown in Fig. 1(b) to permit one crystal face to be an ultrathin membrane, as discussed later.

We choose diamond because diamond crystals have a unique combination of outstanding physical properties that are perfect for many x-ray optics applications for which traditional materials, such as silicon, fail to perform [15]. Single crystals of silicon are attractive because they have an almost perfect crystal lattice, are commercially available in large quantities and are commonly used in x-ray crystal optics. However, many applications, including those considered here, require better performance than silicon can deliver: specifically, better transparency to x-rays, resilience to radiation damage, mechanical stiffness, x-ray Bragg reflectivity and thermal conductivity. Diamond is a material of choice in such cases, as it is superior to silicon because of its unrivaled radiation hardness, an order of magnitude higher transparency to x-rays, an order of magnitude higher stiffness [16, 17], orders of magnitude higher thermal conductivity [18, 19], small thermal expansion [20, 21] and almost 100% reflectivity in Bragg diffraction even in backscattering [22, 23]. This unique combination of outstanding properties makes diamond the most promising

*Electronic address: shvydtko@anl.gov

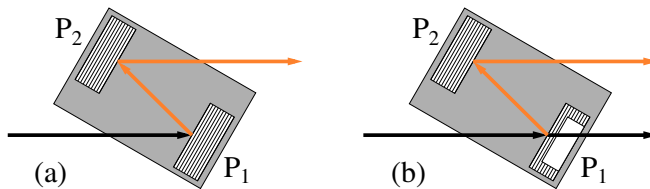


FIG. 1: Schematic of monolithic channel-cut crystals with two reflecting crystal plates P_1 and P_2 . Parallel lines in P_1 and P_2 indicate Bragg-reflecting atomic planes. (a) Standard two-plate channel-cut configuration. (b) design discussed here, featuring a thin crystal membrane in a drumhead structure on plate P_1 . The membrane thickness is sufficient for high Bragg reflectivity in a narrow Bragg-reflection bandwidth and high transmissivity of the out-of-band x-rays.

material for the transparent, resilient, high-resolution, wavefront-preserving x-ray optics components that are essential for many applications at third-generation light sources. These characteristics are especially important at next-generation high-brilliance, high-coherence light sources, such as diffraction-limited storage rings (DLSRs) and XFELs.

The paper is organized as follows. Section II covers the function and optical design of the diamond channel-cut crystals. Details of fabrication are presented in Section III. Results of characterization of the crystals by x-ray rocking curve imaging are presented in Section IV A, and results of x-ray performance tests are given in Section IV B. Conclusions and outlook are discussed in Section V.

II. FUNCTION AND OPTICAL DESIGN

High-repetition-rate (HRR) hard x-ray self-seeded (HXRSS) XFELs will provide x-ray photon beams with an unprecedented spectral flux density advantageous for many applications, in particular for high-resolution spectroscopies, such as nuclear resonant scattering (NRS), inelastic x-ray scattering (IXS) and others. However, dealing with an x-ray beam of such high power is a challenge. Diamond channel-cut crystals can help solve this problem. Our recipe for the solution has four ingredients: a high-indexed Bragg reflection (for a narrow-band reflection), diamond crystal (for x-ray transparency and excellent thermomechanical properties), a drumhead design (for small absorbed power and beam sharing) and a monolithic channel-cut design (for in-line geometry and stability).

An important attribute of high-resolution spectroscopies is the use of x-rays beams with milli-electron volt or even sub-milli-electron volt bandwidths. As a result, such techniques require x-ray sources with large spectral density, and ultra-high-resolution x-ray crystal monochromators with a bandpass of 1–0.1 meV along with submicroradian angular stability; see [24] for a review. Such optics usually cannot perform under high-

heat-load conditions because of the resulting substantial angular instabilities. At storage ring synchrotron radiation facilities, additional primary or high-heat-load crystal monochromators are used [25]. This approach reduces the bandwidth of the undulator x-rays to about 1–2 eV and thus reduces substantially (by a factor of $\simeq 100$) the heat load on the ultra-high-resolution x-ray crystal monochromators.

However, the standard high-heat-load monochromators are not helpful to deal with x-ray beams generated by HRR-HXRSS XFELs, as these sources typically already have a relatively narrow bandwidth of $\simeq 1$ eV. Rather, such beams require a high-resolution monochromator with a bandpass of $\simeq 10$ meV that is stable under high heat loads. This smaller bandpass would reduce the heat load on the ultra-high-resolution optic by a factor of about 100. As an example, 10-keV x-rays can be monochromatized to $\Delta E \simeq 10$ meV with a single Bragg reflection¹. In this case, about 1% of the XFEL radiation power in the small bandwidth can be directed to the ultra-high-resolution monochromator and associated spectroscopic experiments. The remaining 99% of the incident flux is transmitted, rather than being deposited in the crystal, thus avoiding crystal heating, the resulting angular instabilities and, therefore, angular instabilities in the reflected beam. If the monochromator is suitably designed, this remaining flux can be directed to other experiments.

Such multiplexing of the beam requires an x-ray-transparent Bragg-reflecting crystal. Such a crystal would allow most of the incident x-rays, with the exception of the Bragg reflections in the narrow bandwidth, to pass through without absorption. Silicon cannot perform in this way because the 10 extinction lengths required for maximum Bragg reflectivity are comparable to the photoabsorption length in silicon. In contrast, for diamond crystals, 10 extinction lengths equal about 1/10th of the photoabsorption length. Exactly because in diamond the extinction length is much smaller than the absorption length, diamond crystals experience close to 100% Bragg reflectivity, even in backscattering, and simultaneously offer high x-ray transparency [23]. Therefore, we chose to fabricate a diamond crystal membrane with a thickness of about 5 extinction lengths for high x-ray reflectivity and transparency.

However, this dimension of 5 extinction lengths measures only about 20 to 100 μm , depending on the chosen Bragg reflection. It is challenging to fabricate and

¹ XFEL beams typically have a small angular divergence of $\Delta\theta \simeq 2 \mu\text{rad}$ [26, 27]. Because of this property, monochromatization of x-rays to a $\simeq 10$ meV bandwidth can be achieved with a single high-indexed Bragg reflection, because the spectral broadening due to the angular divergence can be kept small ($\delta E/E \simeq \Delta\theta / \tan\theta \lesssim 10^{-6}$), provided Bragg's angle θ is large and $\tan\theta \gg 1$. The use of high-indexed Bragg reflections with θ close to 90° is therefore important.

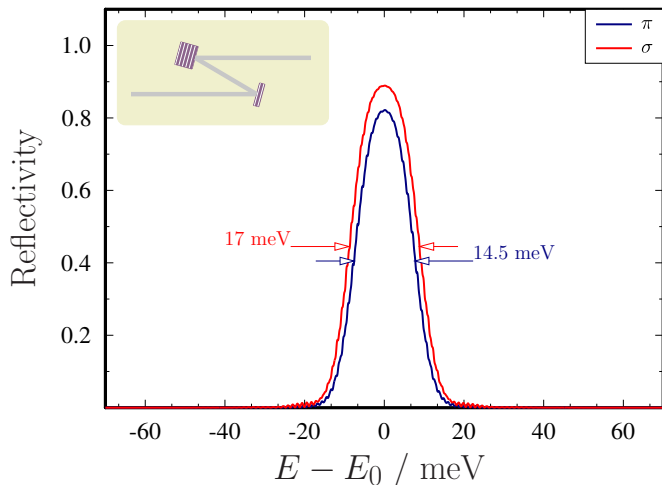


FIG. 2: Calculated x-ray photon energy dependencies for two successive 800 Bragg reflections from a diamond channel-cut crystal. The inset shows the optical setup. The central energy, $E_0 = 14.4125$ keV, corresponds to the nuclear resonance of ^{57}Fe . Bragg's angle is $\theta = 74.7207^\circ$. The spectral dependences are calculated for two possible x-ray polarization states π and σ

handle such ultrathin crystal components without introducing crystal damage and strain. A solution is to use a drumhead crystal: a monolithic crystal structure comprised of a thin membrane furnished with a surrounding solid collar, shown schematically in Fig. 1(b). This design ensures mechanically stable, strain-free mounting of the membrane while still allowing efficient thermal transport [28].

Finally, to ensure a fixed direction of the reflected x-rays independent of Bragg's angle, we add one more equivalent Bragg reflection from another crystal plate in a non-dispersive setting, as shown in Fig. 1. To ensure mechanical stability, both crystal plates are a part of a single, monolithic, channel-cut crystal structure. Channel-cut crystals have been popular in x-ray optics applications since the 1960s [29–32]. Typically they are fabricated from silicon or germanium crystals. Manufacturing a channel-cut crystal from diamond is a challenge, but becomes possible using advanced modern techniques, as discussed in Section III.

In the present discussion, we focus on a diamond monolithic channel-cut crystal for use with 14.4125 keV x-rays for ^{57}Fe nuclear resonant experiments [12, 33, 34]. We also explored a similar design for use with 12.4 keV x-rays for ^{45}Sc experiments [35].

The 733 Bragg reflection in diamond is the highest indexed reflection that is accessible with 14.4-keV x-rays; it has the largest Bragg's angle ($\theta = 80.75226^\circ$) and the smallest Bragg reflection bandwidth (13 meV). However, because of practical considerations related to channel-cut manufacturing (discussed in Section III), we opted for the reflection with the next highest index, the 800 Bragg

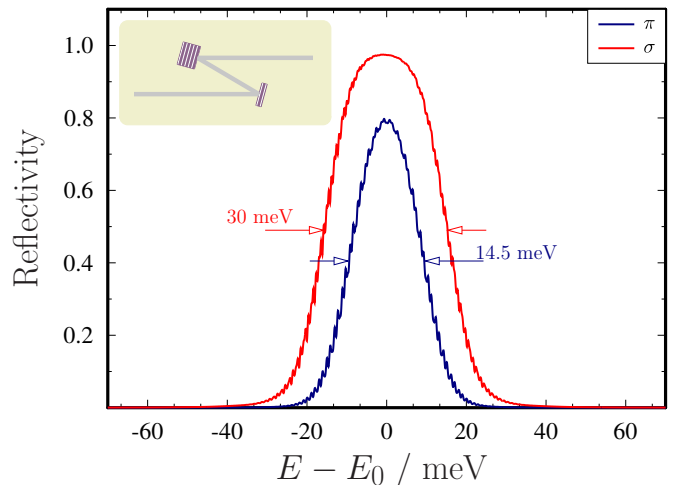


FIG. 3: Calculated x-ray photon energy dependencies for two successive 620 Bragg reflections from a diamond channel-cut crystal. The inset shows the optical setup. The central energy, $E_0 = 12.4$ keV, corresponds to the nuclear resonance in ^{45}Sc . Bragg's angle is 62.424° .

reflection, with a smaller Bragg's angle of $\theta = 74.7207^\circ$ and a larger bandwidth of 20 meV.

Figure 2 shows predicted x-ray photon energy dependencies of the double 800 Bragg reflection profiles from a diamond channel-cut crystal, numerically calculated using equations of dynamical theory of x-ray diffraction in crystals [24, 36]. The first and second reflections are from 50- μm - and 500- μm -thick crystal plates, respectively. The energy bandwidth ΔE is 17 meV for the σ -polarization and 14.5 meV for the π -polarization components of the beam. An angular divergence of the incident x-rays of $2.5 \mu\text{rad}$ is used in the calculations. The calculations show that only 2% of the incident x-ray beam is absorbed in the first plate (the 50- μm -thick diamond drumhead crystal), thus making possible high stability of the monochromator crystal.

Such a diamond monolithic channel-cut crystal can function as a two-bounce 800 Bragg reflection monochromator, deflecting 14.4 keV x-rays within a $\simeq 15$ -meV bandwidth to ^{57}Fe nuclear resonant scattering experiments, while the rest of the x-rays in the 1-eV XFEL bandwidth are transmitted through the thin drumhead crystal and could be transported to a simultaneous experiment ².

Similarly, 620 Bragg reflections are suitable for a diamond channel-cut crystal narrow-band monochromator for 12.4 keV x-rays, corresponding to the nuclear resonance in ^{45}Sc [35]; see Fig. 3.

² To ensure further stability of such a multiplexed setup, it would be advantageous to choose the scattering plane for the diamond channel-cut crystal to be perpendicular to the scattering plane of the downstream ultra-high-resolution optic, as discussed in [7].

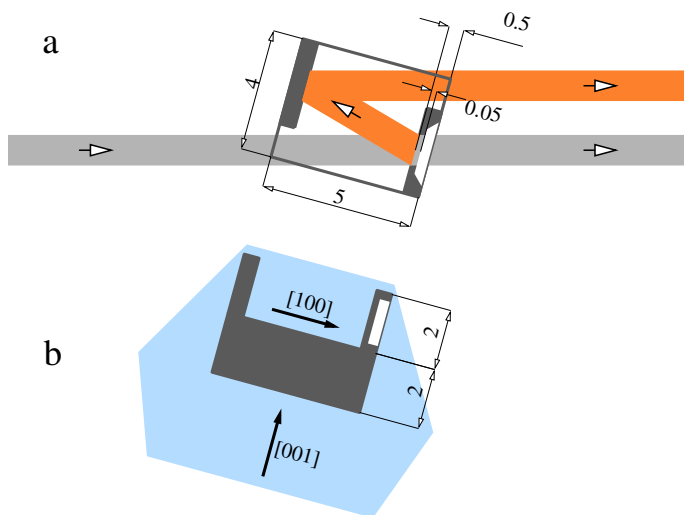


FIG. 4: Schematic of the (800) diamond channel-cut crystal monochromator for 14.4-keV x-rays (black). The channel cut is machined from an as-grown cubo-octahedral diamond crystal stone (light blue). The graph shows top (a) and side (b) views with dimensions in millimeters. Propagation paths of x-ray beams with a 1-mm cross-section are shown in (a).

III. MANUFACTURING

Two conditions are key to successful realization of a properly functioning diamond channel-cut crystal x-ray monochromator: (1) the availability of flawless, single-crystal diamond material in sufficiently large workable sizes and (2) the ability to machine diamond without introducing crystal defects.

The characteristic linear dimensions of presently available high-quality synthetic diamond crystals are in the range of a few millimeters [see [15] for a recent review]. The crystals are relatively small but are sufficient for use with XFEL beams, which are typically less than 1 mm in cross-section. Figure 4 shows a schematic of the diamond channel-cut crystals produced in the present studies.

The channel-cut crystals were cut from synthetically grown raw diamond stones of type IIa (with nitrogen content below 1 ppm). The diamond stones were grown using a temperature gradient method under high pressure and high temperature (HPHT) conditions. The stones used in these studies were grown and machined at the Technological Institute for Superhard and Novel Carbon Materials (TISNCM) in Troitsk, Russia [37, 38].

Raw HPHT-grown diamond stones typically have a cubo-octahedral form. It is well known that the top part of the (001) cubic growth sector (the area furthest from the 001 crystal seed) features the highest crystal quality with lowest defect density [39, 40]. Therefore, in these studies, the channel-cut crystals are extracted from the top part of the stone, as indicated in Fig. 4(b). With this cut, the crystal plate surfaces parallel to the atomic planes (hk0) and to the [001] direction take the largest

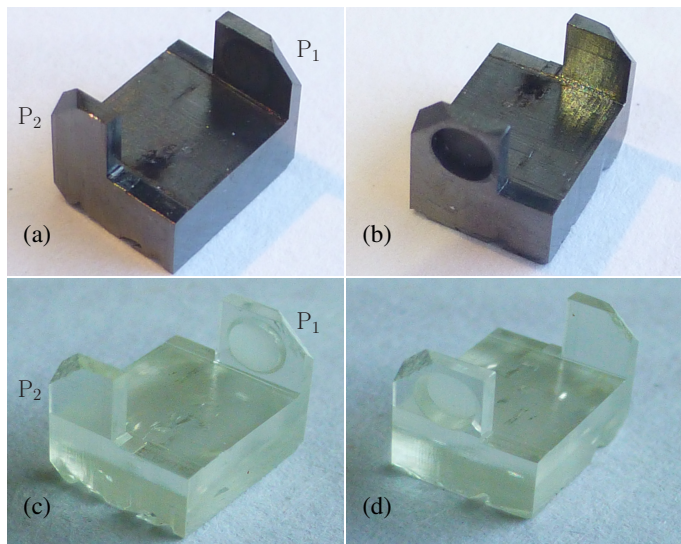


FIG. 5: Photographs of the first (800) channel-cut crystal taken after laser machining (a)-(b) and after annealing in air at 630°C for 3 hours (c)-(d).

volume of highest quality. For this reason, we chose to make a (800) monochromator for use with 14.4 keV x-rays, instead of the narrower band (733) design. Additional reasons for the (800) choice are related to laser machining, as discussed later. Similarly, we chose to make a (620) channel-cut monochromator for 12.4 keV x-rays in the ^{45}Sc case.

Production of the monochromator crystals begins with selection of high-quality, as-grown diamond crystal stones for machining by visual screening. To ensure the fewest defects, crystals with well-developed, defect-free cubic facets are selected, because, as noted previously, the (100) cubic growth sector contains the smallest amount of contamination and structural defects. The diamond stones are machined with the newest laser machining technologies.

The monochromator atomic planes [(800) or (620)] of the selected diamond stones are oriented to an accuracy of better than 0.5° , and the channel-cut crystals are cut to the designed shape using a pulsed Nd:YAG laser with the following parameters: 532 nm wavelength (second harmonic), 15 W average power, 10 kHz repetition rate, ≈ 1.5 mJ pulse energy, 40 ns pulse duration and 15 μm focused spot size (full width half maximum [FWHM]). The laser beam is positioned and steered on the workpiece with a two-coordinate optical mirror scanning system equipped with an F-Theta scanning lens. The laser beam is moved with a linear speed of 100 mm/s.

The drumhead structure is formed by layer-by-layer ablation with picosecond pulses from a Nd:YAG laser operated in the third harmonic (355 nm wavelength) with the following parameters: 1 W average power, 10 ps pulse duration, 500 kHz repetition rate and 2 μJ pulse energy. The use of the third harmonic enables reduction of the focused beam spot size and most importantly reduction

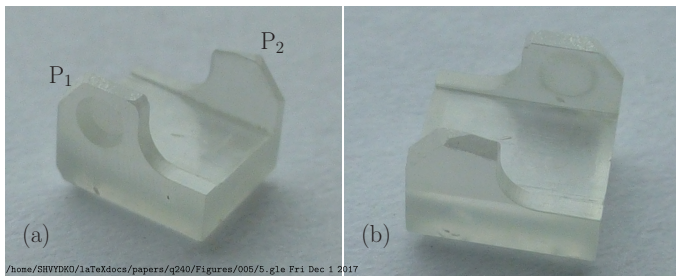


FIG. 6: Photographs of the (620) channel-cut crystal after annealing.

of the diameter of a crater in diamond produced by a single laser pulse. The crater diameter is $8\ \mu\text{m}$, provided the beam is focused on the diamond surface. During ablation, the beam is steered over the workpiece at a speed of $150\ \text{mm/s}$ with a similar two-coordinate scanning system with an F-Theta lens. The removal rate is about $0.3\ \mu\text{m}$ per layer. The surface roughness of the drumhead surface after laser ablation of a 0.5-mm -thick crystal is $\lesssim 1\ \mu\text{m}$ (rms). Similar laser parameters and procedures have been used previously to manufacture diamond x-ray lenses [41] and drumhead crystals [28].

Figure 5(a) shows photographs of the first machined (800) channel-cut crystal. The crystals appear black after machining. Apparently, laser machining is accompanied by graphitization of the diamond surface. To erase the blackening, we anneal the crystals in air at a temperature of $630\text{--}650^\circ\text{C}$ for 3 hours, as in our previous and recent studies [28, 42]. After annealing, the blackening has vanished, as seen on the photographs in Figs. 5(c)-(d). Most important, annealing erases any crystal strain induced in the process of laser cutting or ablation, which is critical for the proper functioning of the channel-cut crystal as a narrow-band x-ray monochromator. The annealing temperature is chosen such that all residuals of graphite and other carbon compounds are burned in air, while keeping diamond intact³. We will refer to this procedure as medium-temperature in-air annealing (MTA).

The first reflecting crystal plate of the channel-cut crystal (P_1 in Fig. 5) features a $50\text{-}\mu\text{m}$ -thick drumhead, designed to achieve high reflectivity ($\gtrsim 90\%$) of x-rays in the Bragg-reflection band and 98% transmissivity of the out-of-band x-rays. X-rays in the 15-meV band reflected from both crystal plates (P_1 and P_2) of the channel-cut crystal (see Fig. 2) are directed to a high-spectral-resolution x-ray instrument. The major part, 98% of the incident x-rays in a 1-eV bandwidth [7, 9], is transmitted and can be used in simultaneous parallel experiments. The 2-mm -thick base allows the crystal to be mounted mechanically tight and strain-free and to be water-cooled efficiently, ensuring stable operation in high-power XFEL

³ Increasing annealing temperature or time may result in etching of the crystal surface.

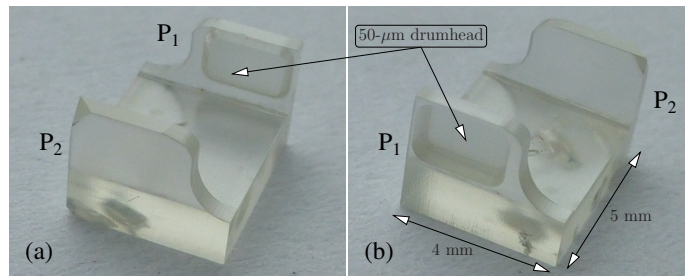


FIG. 7: Photographs of the best-quality (800) channel-cut monochromator crystal (third iteration) after annealing. Note the optimized rectangular shape of the drumhead area.

beams.

Figure 6 shows an example of a (620) diamond channel-cut crystal designed and manufactured for ^{45}Sc nuclear resonant experiments with $12.4\ \text{keV}$ x-rays. The (620) channel-cut crystal also features a $50\text{-}\mu\text{m}$ drumhead on the first plate P_1 . Making drumhead crystals in orientations different from (100) is a challenge [28].

Anisotropy of the physical properties of diamond crystals leads to different results in laser ablation of surfaces with different crystal orientations. Surfaces with the (100) orientation do not present significant problems for laser ablation. In contrast, surfaces with the (111) crystallographic orientation are most difficult both for laser ablation and for polishing. Laser ablation of the (111) surface creates microcracks.

The quality of the (620) surfaces after laser ablation is typically worse than that of the (100) surfaces. We found that increasing the crystal temperature improves the surface quality of the machined surfaces. During machining of the drumhead with the (620) surface orientation, the crystal is heated to 600°C by a resistive heater installed in the crystal holder.

Altogether, three (800) and two (620) channel-cut monochromator crystals were manufactured and characterized. In the following section, we present x-ray characterization results of the best (800) channel-cut crystal monochromator (third iteration), shown in Fig. 7

IV. CHARACTERIZATION OF CHANNEL-CUT CRYSTALS

A. Crystal quality test: X-ray rocking-curve imaging

The quality of the diamond channel-cut crystals was characterized using x-ray Bragg diffraction rocking curve imaging (RCI), also known as sequential topography [43]. In this technique, Bragg reflection images of a crystal under study are measured with a pixel x-ray detector, with images being taken sequentially at different incidence angles to the reflecting atomic planes of the well-collimated x-rays; Bragg reflection maps are calculated

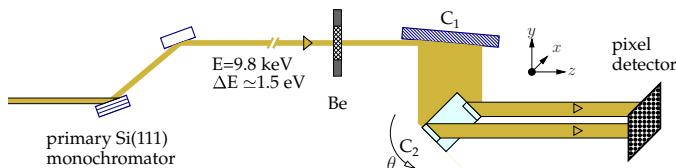


FIG. 8: The layout and optical components of the rocking curve imaging setup at APS bending magnet beamline 1BM, comprising a primary double-crystal Si(111) monochromator, beryllium (Be) window, Si conditioning crystal C_1 in the asymmetric 531 reflection, diamond (800) channel-crystal under study C_2 in the 400 Bragg reflection and pixel detector. X-rays with a 9.8-keV photon energy and a 1.5-eV bandwidth are used.

for the reflection peak intensities, angular widths and angular positions. We used an RCI setup [42, 44] at x-ray optics testing beamline 1BM [45] at the Advanced Photon Source (APS), schematically shown in Fig. 8.

The RCI setup employs a nearly non-dispersive double-crystal C_1 - C_2 arrangement. The first conditioning crystal C_1 is an asymmetrically cut, high-quality silicon crystal in the 531 Bragg reflection; the second crystal C_2 is the structure under study, the (800) diamond channel-cut crystal, in the 400 Bragg reflection. We used the 400 Bragg reflection rather than the 800 reflection to characterize the (800) channel-cut crystal for the following reason. We want both reflecting plates P_1 and P_2 of the channel-cut crystal to be illuminated and imaged simultaneously so that we can evaluate whether there is any angular misorientation of the plates due to crystal defects. To meet this requirement, the Bragg angle must be chosen close to 45° , which in turn would require high-energy (19.66-keV) x-ray photons if the 800 reflection were used. Such a choice would result in time-consuming measurements, as the photon flux is relatively low at this high photon energy, and the angular reflection width ($\Delta\theta_{800} = 1.2 \mu\text{rad}$) is very narrow (compare to $\Delta\theta_{800} = 4.7 \mu\text{rad}$ for 14.4-keV x-rays). Therefore, we chose instead the 400 Bragg reflection and 9.831-keV x-rays, for which Bragg's angle $\theta_{400} = 45^\circ$, with angular width $\Delta\theta_{400} = 9.1 \mu\text{rad}$ if the crystal is 0.5 mm thick (reflecting plate P_1), and $\Delta\theta_{400} = 9.8 \mu\text{rad}$ if the crystal is 0.05 mm thick (drumhead area of reflecting plate P_2).

The upstream double-crystal Si(111) monochromator is therefore tuned to select 9.831-keV x-rays. The monochromator bandwidth is $\simeq 1.5$ eV. For the conditioning crystal C_1 , Bragg's angle is $\theta_{531} = 43.385^\circ$. The asymmetry angle is chosen as $\eta_{531} = 41.4^\circ$, resulting in the asymmetry parameter $b = -28.7$. This choice ensures $\simeq 1 \mu\text{rad}$ angular collimation and a x-ray beam size greater than 20 mm illuminating the channel-cut crystal C_2 . Under these conditions, both plates of the channel-cut crystal are illuminated and can be imaged simultaneously in Bragg diffraction. The setup enables RCI mapping with submicroradian angular and 2.5- μm spatial resolution.

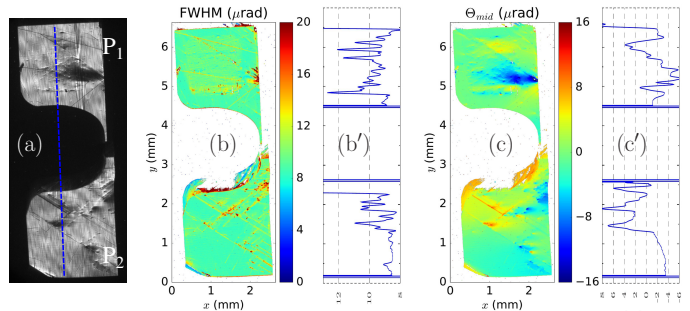


FIG. 9: The 400 Bragg reflection x-ray topography and the RCI maps of the diamond (800) channel-cut crystal measured after second MTA annealing. X-rays illuminate the front face of plate P_1 and the rear face of plate P_2 (drumhead), respectively, corresponding to Fig. 7(a). (a) X-ray topography taken at the peak of the crystal-integrated rocking curve. (b) and (c) Color maps of the Bragg reflection angular widths (FWHM) and mid-point of the Bragg reflection angular curves (rocking curves), respectively. White pixels indicate that the appropriate values of FWHM and mid-point are out of the color scale ranges. (b') and (c') Cross-section profiles of color maps (b) and (c), respectively, measured along the blue line indicated in (a).

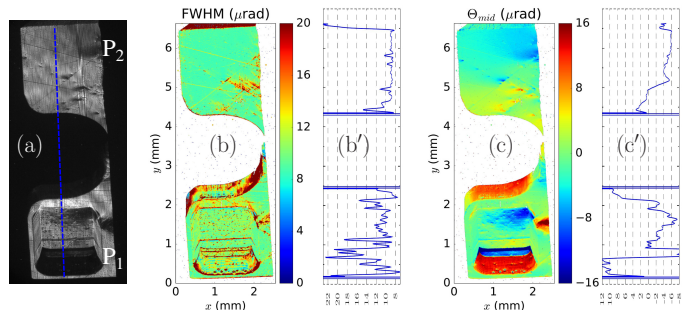


FIG. 10: Similar to Fig. 9, but with the channel-cut crystal exposed to x-rays from the reverse side, corresponding to Fig. 7(b).

X-ray images of the (800) channel-cut crystal taken at the maximum of the sample-integrated Bragg reflection curves are shown in Figs. 9(a) and 10(a). In Fig. 9, x-rays illuminate the front (working) face of plate P_1 and the rear face of plate P_2 , respectively, as in Fig. 7(a). In Fig. 10, the sample is exposed to x-rays from the reverse side, as in Fig. 7(b).

The angular dependencies of Bragg reflectivity (rocking curves) measured with each detector pixel are used to calculate Bragg reflection maps. Figures 9(b) and 10(b) show color maps of the angular widths (FWHM) of the rocking curves. The color maps of the rocking curves' mid-points are shown in Figs. 9(b) and 10(b). The maps are calculated using a dedicated code [46]. Cross-sections through the FWHM and mid-point maps along the blue lines in Figs. 9(a) and 10(a) are presented in Figs. 9(c') and 10(a), respectively.

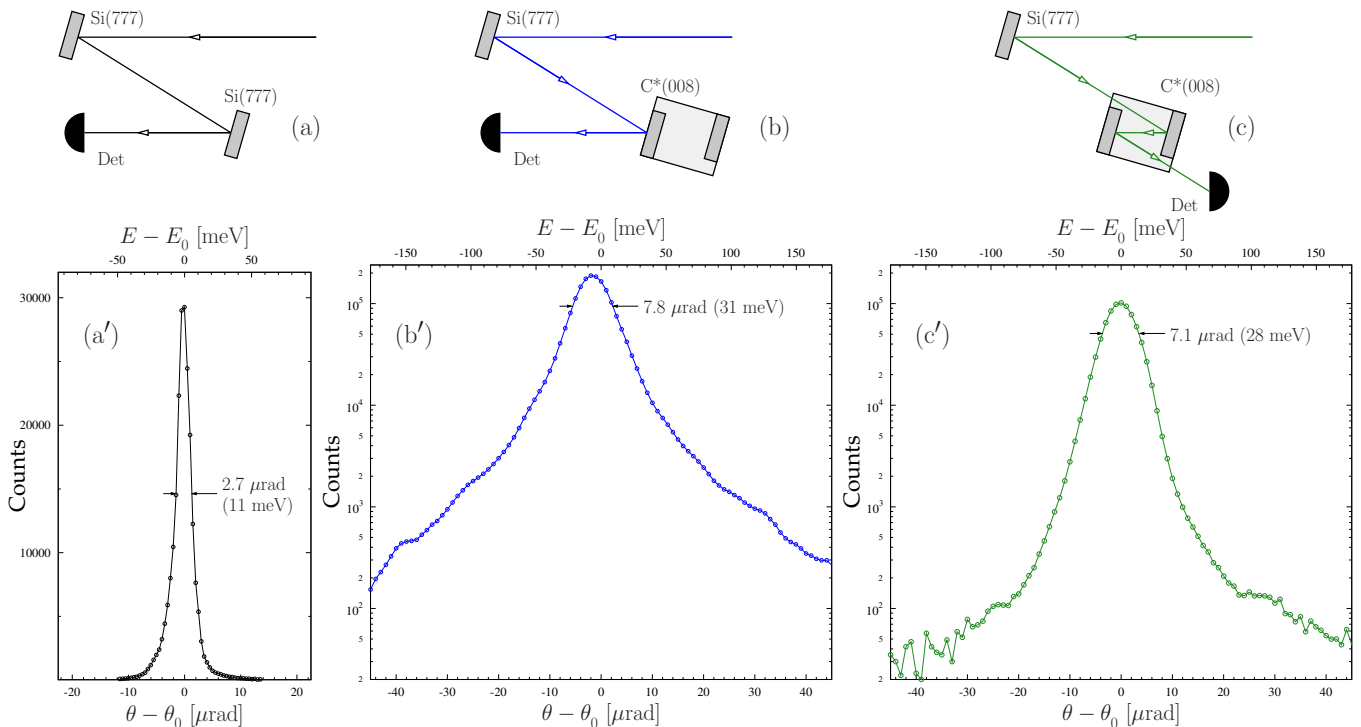


FIG. 11: Schematics of multi-crystal Bragg-diffraction arrangements in non-dispersive settings (a), (b) and (c) to measure the angular dependences of Bragg reflection of 14.41-keV x-rays from (a') a Si(777) crystal, (b') from one (800) plate of the diamond channel-cut crystal, and (c') from both plates sequentially, respectively. In all cases x-rays are first reflected from a Si crystal in the (777) Bragg reflection in a non-dispersive setting with regard to the successive Bragg reflections.

The microscopic defects can be derived from the Bragg reflection FWHM maps. The mesoscopic and macroscopic crystal strain and Bragg planes slope errors can best be evaluated from the mid-point maps. In particular, if the plates of the channel-cut crystal are misoriented due to crystal defects, the mid-point maps will provide this information, because both plates of the channel-cut crystal are imaged simultaneously.

The x-ray images and RCI maps in Figs. 9 and 10 reveal good crystal quality of the manufactured (800) channel-cut crystal, especially in its upper part. Nevertheless, some defects can be detected. These defects result in increased angular widths and varying angular position of the rocking curves. In the center of the plates (in the working area), the angular reflection widths are increased by a few microradians from the expected 9- μ rad angular width of the 400 Bragg reflection. The angular position of the rocking curves also varies within a range of a few microradians, which indicates angular misalignment of the plates. These distortions are caused chiefly by the crystal defects in the as-grown crystal stone. Machining of the diamond has a secondary effect.

B. X-ray performance test: Two-bounce Bragg reflection from the diamond channel-cut crystal

The performance of the manufactured (800) diamond channel-cut crystal was tested by measuring the angular width $\Delta\theta$ of two successive Bragg reflections of x-rays from its crystal plates P_1 and P_2 . The angular width is measured using a non-dispersive double-crystal arrangement, with the first reference crystal chosen to have an angular reflection width much smaller than the angular width of the channel-cut crystal. The spectral width of the channel-cut double reflection can be estimated as $\Delta E/E = \Delta\theta/\tan\theta$ using the differential presentation of Bragg's law and the measured $\Delta\theta$ value.

We used the 777 Bragg reflection of 14.412 keV x-rays from the reference Si crystal with Bragg's angle $\theta_{777} = 73.7848^\circ$ and an angular reflection width of $\Delta\theta_{777} = 1.2 \mu\text{rad}$. It matches well to the 800 Bragg reflection from diamond, with Bragg's angle of $\theta_{800} = 74.7206^\circ$ and an angular width of $\Delta\theta_{800} = 5.2 \mu\text{rad}$.

In the first step, the setup is tested using two successive 777 Bragg reflections from Si crystals, $\text{Si}(777) \times \text{Si}(777)$, as shown schematically in Fig. 11(a). The angular dependence of the Bragg reflection is measured by rocking the angular orientation of the second crystal and thus changing the angle of incidence of x-rays to the diffracting atomic planes. The angular reflection pro-

file shown in Fig. 11(a') features an angular width of $\Delta\theta_a = 2.7 \mu\text{rad}$, which is close to the expected $\simeq 2 \mu\text{rad}$. The additional broadening is attributed to a large horizontal spread of x-rays at a bending magnet beamline. The appropriate spectral bandwidth is calculated to be $\Delta E_a = E\Delta\theta_a / \tan(\theta_{777}) \simeq 11 \text{ meV}$. The angular width $\Delta\theta_a$ and the spectral width ΔE_a represent the angular and spectral resolution of the setup with the reference Si(777) crystal.

In the next step, we used a similar nearly non-dispersive double-crystal Bragg reflection arrangement, Si(777) \times C(800), as shown schematically in Fig. 11(b), to measure the angular width of the single 800 Bragg reflection from one crystal plate of the channel-cut crystal. The reflection profile shown in Fig. 11(b') on a logarithmic scale features an angular width of $\Delta\theta_b = 7.8 \mu\text{rad}$, which is about $\simeq 2.5 \mu\text{rad}$ broader than the expected value. The broadening is attributed to imperfections in the diamond crystal. The appropriate Bragg reflection spectral width calculated from the differential Bragg's law is $\Delta E_b \simeq 31 \text{ meV}$, which should be compared to a 20-meV single-reflection spectral width.

In the final step, we used two successive Bragg reflections from both plates of the (800) channel-cut crystal, as shown schematically in Fig. 11(c), to measure the combined angular Bragg reflection width of the channel-cut crystal. Compared to the single-reflection profile in Fig. 11(b'), the double-reflection profile of the channel-cut crystal, shown in Fig. 11(c') on a logarithmic scale, features steeper tails in the angular profile and a narrower angular width of $\Delta\theta_{bc} = 7.1 \mu\text{rad}$. The appropriate Bragg reflection spectral width calculated from the differential Bragg's law is $\Delta E_a \simeq 28 \text{ meV}$, which is broader than the expected 17-meV (see Fig. 2). The double-reflection peak reflectivity drops by a factor of $\simeq 1.8$ compared to the single-reflection reflectivity in Fig. 11(b'). We attribute the decrease of the double-reflection reflectivity to the angular misorientation of the crystal plates.

Despite the deviations from the theoretical predictions, the manufactured diamond channel-cut crystal is performing within expectations. The experimental data demonstrate the feasibility of using channel-cut diamond crystals to monochromatize x-ray beams at cutting-edge XFELs.

V. CONCLUSIONS AND OUTLOOK

We have demonstrated the feasibility of diamond channel-cut crystals designed to function as high-heat-load, beam-multiplexing, narrow-band, mechanically-stable x-ray monochromators for high-power x-ray beams at cutting-edge, high-repetition-rate XFEL facilities. Laser machining techniques were used to manufacture complex 3D-structures in the channel-cut crystals. The crystals were designed for use as x-ray monochromators for 14.4 keV x-rays, corresponding to the ^{57}Fe nuclear resonance, and for 12.4 keV x-rays, corresponding to the ^{45}Sc nuclear resonance. The channel-cut crystals were characterized by x-ray rocking curve imaging (topography) and by measurement the angular and energy widths of double Bragg reflections. The studied channel-cut crystals perform close to theoretical expectations. However, reflection curves are somewhat broadened, and the channel-cut reflecting plates are misoriented by a few microradians because of crystal defects, which further reduces the double-reflection crystal reflectivity.

High crystal quality in the initial diamond stone used in fabricating the channel-cut crystal is essential for the proper functioning of this diamond monochromator.

Along with applications as monochromators, other applications of the diamond channel-cut crystals are anticipated. In particular, because diamond crystals feature very high x-ray reflectivity, they can be used as efficient four-bounce or six-bounce channel-cut polarizers and analyzers to achieve a very high degree of x-ray polarization purity [47].

VI. ACKNOWLEDGMENTS

Work at Argonne National Laboratory was supported by the U.S. Department of Energy, Office of Science, Office of Basic Energy Sciences, under contract DE-AC02-06CH11357. Diamond crystal growth, quality checks and laser machining at FSBI TISNCM were performed on a Shared-Equipment User Facility "Research of Nanostructured, Carbon and Superhard Materials".

-
- [1] E. L. Saldin, E. A. Schneidmiller, Yu. V. Shvyd'ko, and M. V. Yurkov, Nucl. Instrum. Methods Phys. Res. A **475**, 357 (2001).
 - [2] G. Geloni, V. Kocharyan, and E. Saldin, Journal of Modern Optics **58**, 1391 (2011).
 - [3] J. Amann, W. Berg, V. Blank, F.-J. Decker, Y. Ding, P. Emma, Y. Feng, J. Frisch, D. Fritz, J. Hastings, et al., Nature Photonics **6** (2012).
 - [4] C.-K. Min, I. Nam, H. Yang, G. Kim, C. H. Shim, J. H. Ko, M.-H. Cho, H. Heo, B. Oh, Y. J. Suh, et al., Journal of Synchrotron Radiation **26**, 1101 (2019).
 - [5] I. Inoue, T. Osaka, T. Hara, T. Tanaka, T. Inagaki, T. Fukui, S. Goto, Y. Inubushi, H. Kimura, R. Kinjo, et al., Nature Photonics **13**, 1749 (2019).
 - [6] I. Nam, C.-K. Min, B. Oh, G. Kim, D. Na, H. Y. Young Jin Suh, M. H. Cho, C. Kim, M.-J. Kim, C. H. Shim, et al., Nature Photonics **X**, X (2021).
 - [7] O. Chubar, G. Geloni, V. Kocharyan, A. Madsen, E. Saldin, S. Serkez, Yu. Shvyd'ko, and J. Sutter, Journal of Synchrotron Radiation **23**, 410 (2016).

- [8] X. Yang and Yu. Shvyd'ko, Phys. Rev. ST Accel. Beams **16**, 120701 (2013).
- [9] G. Geloni, V. Kocharyan, and E. Saldin, arXiv:1508.04339 (2015), DESY 15-141.
- [10] A. Q. R. Baron, *Synchrotron Light Sources and Free-Electron Lasers* (Springer International Publishing, Switzerland, 2016), chap. "High-Resolution Inelastic X-Ray Scattering", pp. 1643–1757.
- [11] O. G. Shpyrko, Journal of Synchrotron Radiation **21**, 1057 (2014).
- [12] R. Ruffer and A. Chumakov, *Synchrotron Light Sources and Free-Electron Lasers* (Springer International Publishing, Switzerland, 2016), chap. "Nuclear Resonance", pp. 1–32.
- [13] W. Decking, S. Abeghyan, P. Abramian, and et al., Nature Photonics **14**, 391 (2020).
- [14] T. Raubenheimer, in *Proc. 60th ICFA Advanced Beam Dynamics Workshop (FLS'18), Shanghai, China, 5-9 March 2018* (JACoW Publishing, Geneva, Switzerland, 2018), no. 60 in ICFA Advanced Beam Dynamics Workshop, pp. 6–11, ISBN 978-3-95450-206-6, <https://doi.org/10.18429/JACoW-FLS2018-MOP1WA02>, URL <http://jacow.org/fls2018/papers/mop1wa02.pdf>.
- [15] Yu. Shvyd'ko, V. Blank, and S. Terentyev, MRS Bulletin **62**, 437 (2017).
- [16] J. E. Field, ed., *The Properties of Natural and Synthetic Diamond* (Academic Press, 1992).
- [17] M. A. Prelas, G. Popovici, and L. K. Bigelow, eds., *Handbook of Industrial Diamonds and Diamond Films* (Marcel Dekker, Inc., New-York, 1998).
- [18] L. Wei, P. K. Kuo, R. L. Thomas, T. R. Anthony, and W. F. Banholzer, Phys. Rev. Lett. **70**, 3764 (1993).
- [19] A. V. Inyushkin, A. N. Taldenkov, V. G. Ralchenko, A. P. Bolshakov, A. V. Koliadin, and A. N. Katrusha, Phys. Rev. B **97**, 144305 (2018), URL <https://link.aps.org/doi/10.1103/PhysRevB.97.144305>.
- [20] S. Stoupin and Yu. V. Shvyd'ko, Phys. Rev. Lett. **104**, 085901 (2010).
- [21] S. Stoupin and Yu. V. Shvyd'ko, Phys. Rev. B **83**, 104102 (2011).
- [22] Yu. V. Shvyd'ko, S. Stoupin, A. Cunsolo, A. Said, and X. Huang, Nature Physics **6**, 196 (2010).
- [23] Yu. V. Shvyd'ko, S. Stoupin, V. Blank, and S. Terentyev, Nature Photonics **5**, 539 (2011).
- [24] Yu. Shvyd'ko, *X-Ray Optics – High-Energy-Resolution Applications*, vol. 98 of *Optical Sciences* (Springer, Berlin, 2004).
- [25] A. I. Chumakov, I. Sergeev, J.-P. Celse, R. Ruffer, M. Lesourd, L. Zhang, and M. Sánchez del Río, Journal of Synchrotron Radiation **21**, 315 (2014).
- [26] E. L. Saldin, E. A. Schneidmiller, and M. V. Yurkov, *The Physics of Free Electron Lasers*, Advanced Texts in Physics (Springer, Berlin Heidelberg, 2000).
- [27] Z. Huang and K.-J. Kim, Phys. Rev. ST Accel. Beams **10**, 034801 (2007).
- [28] T. Kolodziej, P. Vodnala, S. Terentyev, V. Blank, and Yu. Shvyd'ko, Journal of Applied Crystallography **49**, 1240 (2016).
- [29] U. Bonse and M. Hart, Appl. Phys. Lett. **6**, 155 (1965).
- [30] U. Bonse and M. Hart, Z. Physik **188**, 154 (1965).
- [31] U. Bonse and M. Hart, Z. Physik **189**, 151 (1966).
- [32] R. D. Deslattes, Appl. Phys. Lett. **12**, 133 (1968).
- [33] E. Gerdau and H. de Waard, eds., *Nuclear Resonant Scattering of Synchrotron Radiation* (Baltzer, 1999/2000), special issues of the *Hyperfine Interact.*, Vol. 123-125.
- [34] R. Röhlberger, *Nuclear Condensed Matter Physics with Synchrotron Radiation. Basic Principles, Methodology and Applications*, vol. 208 of *Springer Tracts in Modern Physics* (Springer Verlag, Berlin-Heidelberg, 2004).
- [35] Yu. V. Shvyd'ko and G. V. Smirnov, Nucl. Instrum. Methods Phys. Res. B **51**, 452 (1990).
- [36] A. Authier, *Dynamical Theory of X-Ray Diffraction*, vol. 11 of *IUCr Monographs on Crystallography* (Oxford University Press, Oxford, New York, 2001).
- [37] V. Blank, M. Kuznetsov, S. Nosukhin, S. Terentiev, and V. Denisov, Diamond and Related Materials **16**, 800 (2007).
- [38] S. N. Polyakov, V. N. Denisov, N. V. Kuzmin, M. S. Kuznetsov, S. Y. Martyushov, S. A. Nosukhin, S. A. Terentiev, and V. D. Blank, Diamond and Related Materials **20**, 726 (2011).
- [39] R. C. Burns, A. I. Chumakov, S. H. Connell, D. Dube, H. P. Godfried, J. O. Hansen, J. Härtwig, J. Hoszowska, F. Masiello, L. Mkhonza, et al., J. Phys.: Condensed Matter **21**, 364224(14pp) (2009).
- [40] H. Sumiya and K. Tamasaku, Jpn. J. Appl. Phys. **51**, 090102 (2012).
- [41] S. Terentyev, V. Blank, S. Polyakov, S. Zholudev, A. Snigirev, M. Polikarpov, T. Kolodziej, J. Qian, H. Zhou, and Yu. Shvyd'ko, Appl. Phys. Lett. **107**, 111108 (2015).
- [42] P. Pradhan, M. Wojcik, X. Huang, E. Kasman, L. Assoufid, J. Anton, D. Shu, S. Terentyev, V. Blank, K.-J. Kim, et al., Journal of Synchrotron Radiation **27**, 1553 (2020).
- [43] D. Lübbert, T. Baumbach, J. Härtwig, E. Boller, and E. Pernot, Nucl. Instrum. Methods Phys. Res. B **160**, 521 (2000).
- [44] S. Stoupin, Yu. Shvyd'ko, E. Trakhtenberg, Z. Liu, K. Lang, X. Huang, M. Wiczorek, E. Kasman, J. Hammonds, A. Macrander, et al., AIP Conf. Proc. **1471**, 050020 (2016).
- [45] A. Macrander, M. Erdmann, N. Kujala, S. Stoupin, S. Marathe, X. Shi, M. Wojcik, D. Nocher, R. Conley, J. Sullivan, et al., in *AIP Conf. Proc.* (2016), vol. 1741, p. 030030, ISBN 9780735413986, ISSN 15517616.
- [46] S. Stoupin (2015), URL <https://www1.aps.anl.gov/science/scientific-software/dtxrd>.
- [47] H. Bernhardt, B. Marx-Glowna, K. Schulze, B. Grabiger, J. Haber, C. Detlefs, R. Löttsch, T. Kämpfer, R. Röhlberger, E. Förster, et al., Applied Physics Letters **109**, 121106 (2016).